Preprints.org

Article

Not peer-reviewed version

# Tribological Behavior of Cotton Fabric/Phenolic Resin Laminated Composites Reinforced with Two-Dimensional Materials

Yonggang Guo , Chenyang Fang , Tingmei Wang , Qihua Wang , Fuzhi Song * , Chao Wang *

Posted Date: 20 October 2023

doi: 10.20944/preprints202310.1311.v1

Keywords: two-dimensional materials; cotton fabric; phenolic resin; friction and wear; molecular dynamics

Preprints.org is a free multidiscipline platform providing preprint service that is dedicated to making early versions of research outputs permanently available and citable. Preprints posted at Preprints.org appear in Web of Science, Crossref, Google Scholar, Scilit, Europe PMC.

Copyright: This is an open access article distributed under the Creative Commons Attribution License which permits unrestricted use, distribution, and reproduction in any medium, provided the original work is properly cited.

*Preprints* (www.preprints.org) | NOT PEER-REVIEWED | Posted: 20 October 2023 doi:10.20944/preprints202310.1311.v1

Disclaimer/Publisher's Note: The statements, opinions, and data contained in all publications are solely those of the individual author(s) and contributor(s) and not of MDPI and/or the editor(s). MDPI and/or the editor(s) disclaim responsibility for any injury to people or property resulting from any ideas, methods, instructions, or products referred to in the content.

*Article*

# Tribological Behavior of Cotton Fabric/Phenolic Resin Laminated Composites Reinforced with Two-Dimensional Materials

**Yonggang Guo [1], Chenyang Fang [1], Tingmei Wang [2], Qihua Wang [2], Fuzhi Song [2,3]* and Chao Wang [2,3]***

[1] School of Mechanical and Electrical Engineering, Henan University of Technology, Zhengzhou, 450001, China
[2] Key Laboratory of Science and Technology on Wear and Protection of Materials, Lanzhou Institute of Chemical Physics, Chinese Academy of Sciences, Lanzhou, 730000, China
[3] Qingdao Center of Resource Chemistry & New Materials, Qingdao, 266071, China
* Correspondence: fuzsong@licp.cas.cn (F.S.); wangc@licp.cas.cn (C.W.)

**Abstract:** In this study, cotton fabric reinforced phenolic resin (CPF) composites were modified by adding four two-dimensional fillers: graphitic carbon nitride (g-$C_3N_4$), graphite (Gr), molybdenum disulfide ($MoS_2$), and hexagonal boron nitride (h-BN). The tribological properties of these modified materials were investigated under dry friction and water lubrication conditions. CPF/ Gr composite exhibits significantly better tribological performance than the other three fillers modified CPF composites under dry friction, with a 24% reduction in friction coefficient and a 78% reduction in wear rate compared to unmodified CPF composite. Under water lubrication conditions, all four fillers did not significantly alter the friction coefficient of the CPF composite. However, except for an excessive amount of Gr, the other three fillers can reduce the wear rate. Particularly, in the case of 10% $MoS_2$ content, the wear rate decreased by 56%. Scanning electron microscopy (SEM) and X-ray photoelectron spectroscopy (XPS) were employed for the analysis of the morphology and composition of the transfer films. Additionally, molecular dynamics (MD) simulations were conducted to investigate the adsorption effects of Gr, $MoS_2$, and PF on the counterpart surface under both dry friction and water lubrication conditions. The difference in the adsorption capacity of Gr and $MoS_2$ on the counterpart, as well as the resulting formation of transfer films, accounts for the variation in tribological behavior between CPF/Gr and CPF/$MoS_2$ composites. By combining the lubrication properties of $MoS_2$ and Gr under dry friction and water lubrication conditions, using them as co-fillers can achieve a synergistic lubrication effect.

**Keywords:** two-dimensional materials; cotton fabric; phenolic resin; friction and wear; molecular dynamics

## 1. Introduction

Oil-lubricated stern bearings have the risk of oil leakage and combustion in the process of use, and are prone to wear and damage due to dry friction when the oil is cut off[1]. With the growing environmental awareness and stricter pollution standards, people are urged to research and develop new bearing systems that are pollution-free, wear-resistant, efficient, energy-saving, and long-lasting and so on[2-4]. Water is the most promising lubricating medium due to its non-pollution, wide source, safety, and incombustibility properties[5, 6]. However, there is a significant difference in the physical properties between water and lubricating oil[7]. Compared to lubricating oil, water has low viscosity, making it difficult to form a lubricating film on the friction interface. Especially in the frequent starting and stopping and variable load conditions, the lubrication between the shaft and the bearing is mixed lubrication, boundary lubrication, or dry friction conditions occur, which seriously reduced the safety and life of the stern bearing[8-11]. Therefore, it is very necessary to develop materials with excellent anti-friction and anti-wear properties in a water environment for addressing the limitations of water lubrication and improving the service life of bearings.

High-performance fiber fabric-reinforced resin composites combine advantage of both fibers and resins, making them a high-strength low self-lubricating bearing material[12-15]. Among them, the properties of the resin matrix play a crucial role in the overall tribological performance of the

© 2023 by the author(s). Distributed under a Creative Commons CC BY license.

Preprints (www.preprints.org) | NOT PEER-REVIEWED | Posted: 20 October 2023 doi:10.20944/preprints202310.1311.v1



composites[16]. Phenolic resin (PF) has the advantages of good mechanical properties, dimensional stability, simple production process, and wear resistance, and is often used as adhesive resin[17-19]. Despite the excellent properties of fiber fabric-reinforced PF composites, there are still some challenges in terms of friction and wear. This is not only manifested by the fact that pure PF has a high coefficient of friction, significant friction noise, and poor dimensional stability when exposed to moisture[20, 21]. On the other hand, due to the low chemical reactivity of the fiber fabric surface and poor adhesion between the fibers and the resin, during the friction process, the resin and fibers are prone to debonding, resulting in a sharp increase in the wear of the composite material[22]. Therefore, it is of great importance to improve the friction and wear properties of phenolic resins.

Modification of polymer resins by filler blending has become a common method to improve the tribological properties of fabric composites[23-25]. Expect nanoparticles, such as Si3N4、CaCO3、TiO2、CuO、Al2O3、ZnO、SiC, two-dimensional materials have been increasingly used in the field of solid lubrication, either individually or in combination with other substances, due to their unique layered structure, high mechanical strength, low shear resistance, and structural flexibility[26, 27]. The crystal structure of g-C3N4 has the strong covalent C-N bonds and weak van der Waals forces between layers, which has excellent lubricity properties similar to those of carbon-based nanomaterials. Wu et al[28]. filled the prepared g-C3N4 nanosheets into a phenolic resin coating and investigated the effect on its tribological properties, suggesting that the modified tribological properties of g-C3N4 nanosheets may be attributed to its lamellar structure and high specific area contributing to the formation of a thin and continuous transfer film. Zhang et al[29]. investigated the influence of graphite, graphene, and graphene oxide fillers on the tribological performance of PTFE/Nomex hybrid fabric/phenolic resin composites, and revealed that all three solid lubricant fillers were effective in reducing the wear rate of the fabric composites. The hexagonal boron nitride (h-BN), so-called “white graphite” due to it crystalline structure analogous to graphite, consists of a honeycomb structure with alternating bound boron and nitrogen atoms, which possesses extremely high resistance to oxidation, thermal conductivity and self-lubricating properties[30]. Gao et al[10]. obtained significantly improved tribological performance by adding h-BN nanoparticles into polyoxymethylene (POM) composite. MoS2 is an advanced lubricating material, but the characteristics of low shear strength of MoS2 would be reduced in a humid environment[31]. However, more recent studies demonstrated that MoS2 could still maintain the capacity of lubrication in aqueous lubrication. Xin et al[32]. prepared MoS2/PEEK composites using ball milling and spark plasma sintering processes, and the experimental results showed that MoS2/PEEK composites have excellent anti-wear properties under water lubrication conditions, and are a potential material for underwater equipment.

Currently, there have been reports on the tribological properties of modified fiber fabric composites. However, most of these studies focus on PTFE fibers and Nomex fibers, while there is limited research on cotton fabric reinforced phenolic resin (CPF) composites. Considering that CPF composites remain the most widely used type of water-lubricated bearing material, further research on their modification to enhance friction and wear performance and overcome the performance limitations of current water-lubricated bearing materials is of significant practical value.

In this study, CPF composites were modified by adding different proportions of four two-dimensional materials: g-C3N4, graphite (Gr), MoS2, and h-BN. The tribological properties of these modified materials were investigated under dry friction and water lubrication conditions. Based on the experimental results, molecular dynamics simulations were employed to calculate the adsorption energy between the CPF composites filled with Gr and MoS2 and the counterpart surfaces at the microscopic scale. This analysis effectively explains the reasons for the contrasting tribological performance of Gr and MoS2 fillers in different environments. The findings of this research provide theoretical guidance for the frictional modification of CPF materials.

Preprints (www.preprints.org) | NOT PEER-REVIEWED | Posted: 20 October 2023 doi:10.20944/preprints202310.1311.v1



## 2. Experimental

### *2.1. Materials*

The adhesive resin (2127 phenolic resin) was provided by Wuxi YinyeHao Chemical Co., Ltd. Cotton fabric is woven from 100-count cotton yarn. Molybdenum disulfide (MoS2, particle size 12-16μm, ≥99.9%) was provided by Shanghai Macklin Biochemical Technology Co., Ltd. Hexagonal boron nitride (h-BN, particle size 5-10μm, ≥99.9%) was provided by Shanghai Macklin Biochemical Technology Co., Ltd. Graphite (Gr, particle size 5-10μm, ≥99%) was provided by Shanghai Meryer Chemical Technology Co., Ltd. Anhydrous ethanol was provided by Qingdao SankaiMedical Technology Co. Ltd. The g-C3N4 was synthesized by calcination method, and the other chemical agents used as received without further treatment. The powder was used to ultrasonic treatment before use, and the particle size distribution after ultrasonication is shown in Figure 2d.

The preparation process of the g-C3N4 is shown as follows[33]: Firstly, melamine powder was put into an alumina crucible with a lid, ramped at 10 °C/ min to 550 °C, where it was held for 2 h and then cooled to room temperature. The collected yellow products were dry rubbed in a ball mill for 12 hours, then the graphitic phase carbon nitride (g-C3N4) was obtained.

### *2.2. Sample Preparation*

Firstly, the cotton fabric was cut into 70cm×20cm for later use. The four fillers were added into the PF resins solution in the proportion shown in Table 1. The mixture is vigorously stirred using a high-speed mixer for 1 hour to ensure the fillers are uniformly blended in the resin solution. Subsequently, the mixture is further processed with a three-roller calender to ensure even dispersion of the four fillers. The dispersed resin solution stirred at high speed for 1h. Subsequently, the cotton fabric was submerged in the pre-prepared resin solution and subjected to ten minutes of ultrasonic treatment. The immersion was repeated several times until the relative mass fraction of the resin mixture reached 60±5%, and then placed in an oven at 110°C for a three-minute drying period.

The obtained impregnated fabric was cut into 85 mm × 50 mm pieces, which were stacked layer by layer and then placed into the mold. The fabrication of CPF composites were carried out using a hot-pressing process, with curing at 2.6 MPa and 130°C for 4h. Finally, the CPF composites were taken out and cut into 25 mm ×10 mm × 3 mm to make the test samples.

**Table 1.** Designations and detailed compositions (wt.%) of CPF composites.

| Composites/wt% | PF | g-$C_3N_4$ | Gr | $MoS_2$ | h-BN |
|---|---|---|---|---|---|
| CPF | 100 | / | / | / | / |
| CPF/3CN | 97 | 3 | / | / | / |
| CPF/5CN | 95 | 5 | / | / | / |
| CPF/10CN | 90 | 10 | / | / | / |
| CPF/15CN | 85 | 15 | / | / | / |
| CPF/3Gr | 97 | / | 3 | / | / |
| CPF/5Gr | 95 | / | 5 | / | / |
| CPF/10Gr | 90 | / | 10 | / | / |
| CPF/15Gr | 85 | / | 15 | / | / |
| CPF/3$MoS_2$ | 97 | / | / | 3 | / |
| CPF/5$MoS_2$ | 95 | / | / | 5 | / |
| CPF/10$MoS_2$ | 90 | / | / | 10 | / |
| CPF/15$MoS_2$ | 85 | / | / | 15 | / |
| CPF/3BN | 97 | / | / | / | 3 |
| CPF/5BN | 95 | / | / | / | 5 |
| CPF/10BN | 90 | / | / | / | 10 |
| CPF/15BN | 85 | / | / | / | 15 |

Preprints (www.preprints.org) | NOT PEER-REVIEWED | Posted: 20 October 2023 doi:10.20944/preprints202310.1311.v1



*2.3. Tribological Tests*

Tribological tests were carried out using a block-on-ring apparatus (MRH-1A, Jinan Yihua Tribology Testing Technology Co, Ltd.). The structure of the friction pair is shown in Figure 1a. The test samples had a dimension of 25×10×3mm$^3$. GCr15 and QSn7-0.2 were selected as the counterparts under dry friction and water lubrication conditions, respectively. GCr15 steel is frequently used as bearing steel, and has excellent mechanical properties but poor corrosion resistance in water lubrication, while QSn7-0.2 is used in the water environment due its excellent corrosion resistance[34]. The diameter of the counterpart ring was 49.95± 0.05mm. The surface of the ring was polished with SiC metallographic abrasive papers and the mean roughness Ra was controlled about 0.2μm with random distributed grooves as shown in Fig. 1b, c. The counterpart ring was thoroughly cleaned with petroleum ether in an ultrasonic bath for 10 min before test.

All the tribological tests were conducted at room temperature. For water lubrication, both the specimen and the counterpart were fully immersed in pure water. A constant normal load of 132N was applied throughout the tests. The tribological experiments were performed at a constant and variable sliding speeds, respectively. In the variable-speed friction experiment, the rotation speeds ranged from 35 to 1120 rpm, corresponding to velocities of 0.09 m/s, 0.18 m/s, 0.36 m/s, 0.73 m/s, 1.47 m/s and 2.93 m/s. The speed was increased every 30 minutes, and the total duration of the experiment was 180 minutes. In the constant-speed friction experiment, the rotation speed was set at 140 rpm (0.36m/s), and the experiment lasted for 120 minutes. Every test was repeated three times, using the average value as the test result. The friction coefficient (COF) was automatically recorded by the tribometer. The specific wear rate of the test samples was calculated according to Eq. (1)[35].

$$W_S = \frac{B}{L \times F}\left[R^2 \arcsin\left(\frac{W}{2R}\right) - \frac{W}{4}\sqrt{4R^2 - W^2}\right] (\mathrm{mm^3/Nm}) \quad (1)$$

where B is the width of polymer testing samples, R is the radius of counterpart ring, W is the projected width of the wear track (depending on material loss), F is the normal load applied on polymer samples (132 N), and L is the total sliding distance (m).

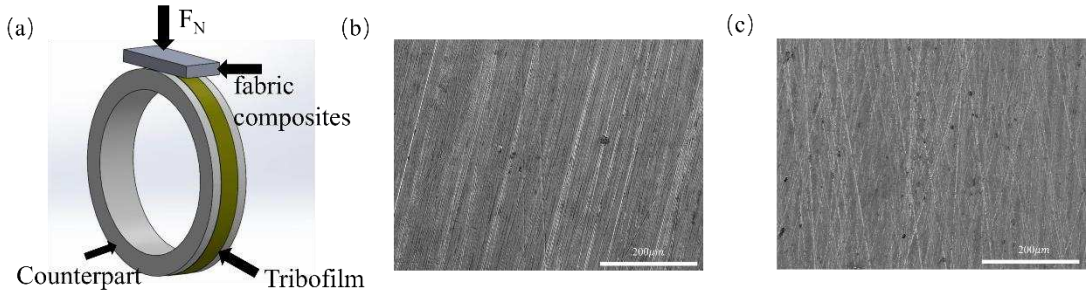


**Figure 1.** (a) Schematic diagram of block-on-ring wear tester; (b) SEM images of GCr15 surface; (c) SEM images of QSn7-0.2 surface.

*2.4. Testing and Characterization*

The particle size of the four fillers after ultrasonic treatment was measured using a laser particle size distribution meter (LF-POP, Omicron). X-ray diffraction (XRD, SmartLab9KW) and Fourier transform infrared spectroscopy (FTIR, Bruker) were used to observe the chemical structure composition of g-$C_3N_4$. Scanning electron microscope (SEM, JSM-7610F) were used to investigated the surface microscopy of the counterparts and the worn surface of fabric composites. The changes in the phase composition and chemical composition of the worn surface of counterparts were examined using an X-ray photoelectron spectroscopy (XPS, Thermo Fisher Scientific).

Preprints (www.preprints.org) | NOT PEER-REVIEWED | Posted: 20 October 2023 doi:10.20944/preprints202310.1311.v1



## 3. Results and Discussion

### *3.1. Characterization of g-$C_3N_4$ and Particle Size Distribution of Four Fillers*

Figure 2a shows the g-$C_3N_4$ XRD pattern, it can be seen that two major diffraction peaks appear near 13.1 and 27.3, and no diffraction peaks of other impurity phases were detected in all samples. The peaks located at 13.1° and 27.5° were attributed to the (100) and (002) planes, which were respectively related to the interlayer structural packing and interlayer stacking structure[26]. The molecular structure of g-$C_3N_4$ was further confirmed by the FTIR spectroscopy, as shown in Fig. 2b. The broad bands in the 3000-3500 $cm^{-1}$ were attributed to the secondary (=NH) and primary (-$NH_2$) amines. Noticeably, the set of peaks between 1200 $cm^{-1}$ and 1700 $cm^{-1}$ can be assigned to the typical stretching vibration of CN heterocycles. The distinct and sharp peak at around 807 $cm^{-1}$ was originated from representative tri-s-triazine units[28]. These observations confirm the successful synthesis of g-$C_3N_4$. Figure 2c shows morphology of the synthesized g-$C_3N_4$ powder. It can be seen that g-$C_3N_4$ powder exhibits an irregular flake-like structure. Particle sizes of g-$C_3N_4$, Gr, $MoS_2$, and h-BN used as filler to modify the CPF composites were tested using laser particle size distribution instrument, as shown in Figure 2d, the particle sizes of these four fillers are similar, with an average particle size ranging from 0.7 to 2.5μm.

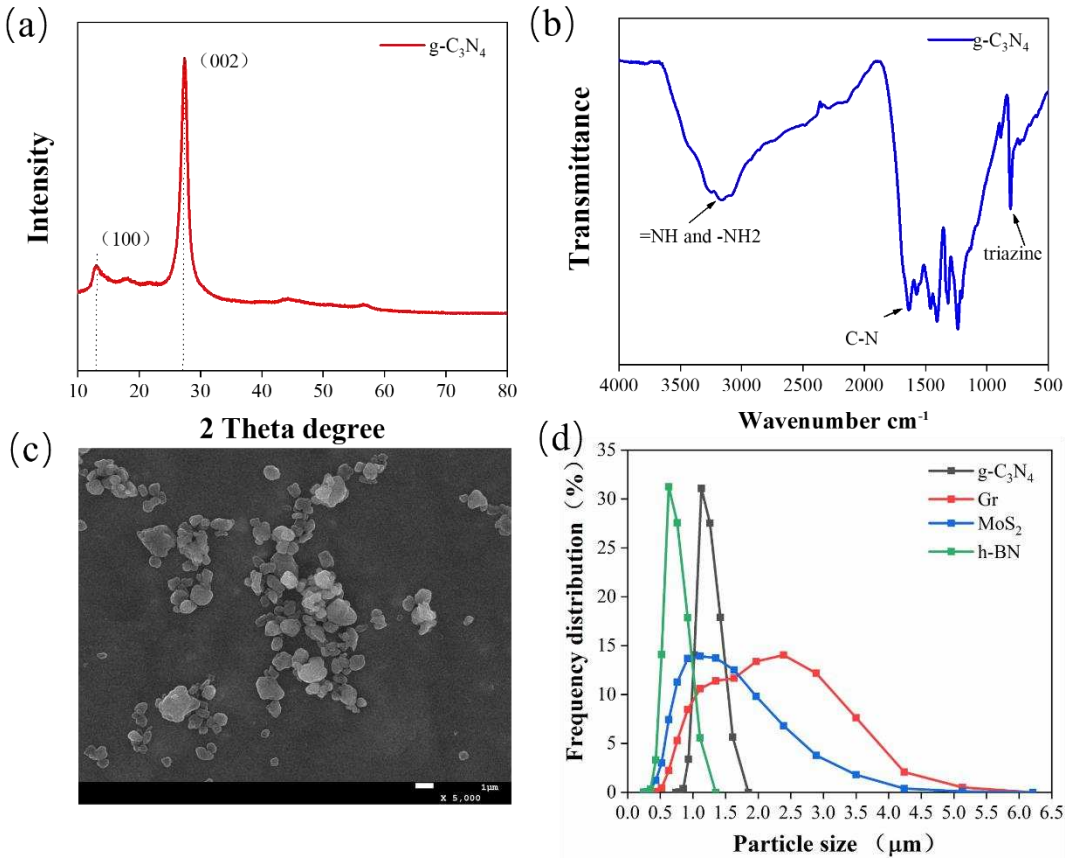


**Figure 2.** (a) XRD patterns of g-$C_3N_4$; (b) FTIR spectra of g-$C_3N_4$; (c)SEM micrograph of g-$C_3N_4$; (d) the particle size of the four fillers.

### *3.2. Tribological Properties*

#### 3.2.1. Tribological Behaviors at Varying Sliding Speeds under Water Lubrication

Figure 3a shows the friction coefficient curve of unmodified and four types of two-dimensional material-modified CPF composites with a mass fraction of 15%. The applied load is 132N, and the sliding speed increases from 0.09 m/s to 2.93 m/s, with a change in speed every 30 minutes. It can be seen that in the initial stages of friction, several CPF composites undergo a noticeable running-in

Preprints (www.preprints.org) | NOT PEER-REVIEWED | Posted: 20 October 2023 doi:10.20944/preprints202310.1311.v1



process where the friction coefficient gradually increases and then stabilizes. As the velocity continues to increase, the friction coefficient of all CPF composites decreases with higher speeds. At lower speeds, compared to unmodified CPF composites, the friction coefficient of $MoS_2$ and g-$C_3N_4$ modified CPF composites is relatively higher. However, when the velocity exceeds 0.36 m/s, the friction coefficient of these CPF composites significantly decreases, and it becomes lower than that of unmodified CPF composites.

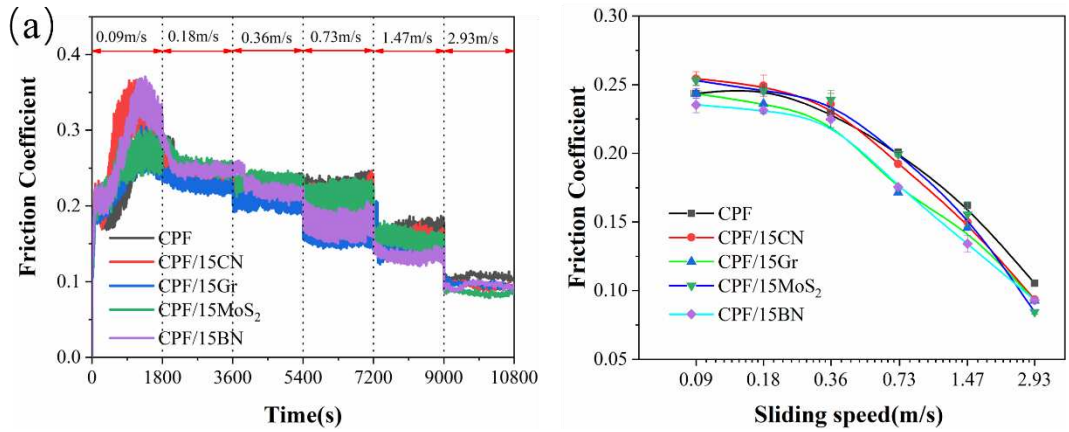


**Figure 3.** (a) Friction coefficient of CPF, CPF/15CN, CPF/15Gr, CPF/15$MoS_2$ and CPF/15BN as the function of sliding speed; (b) Stribeck curves derived from friction coefficients of various speed steps. Load: 132N, Lubrication medium: pure water.

The friction coefficient curves plotted based on the average values of friction coefficients within different velocity ranges are shown in Figure 3b. It can be observed that during the variable speed process, all five CPF composites exhibit typical Stribeck curve characteristics. This means that as the velocity increases, the friction system gradually transitions from boundary lubrication to mixed lubrication. However, throughout the entire process, the friction coefficients are noticeably higher than those under conventional water lubrication conditions. These results indicate that the friction interface is not purely in a state of either boundary lubrication or mixed lubrication; instead, it involves dry friction. This is mainly because the phenolic resin composites are relatively hard, and the contact load at the friction interface is significant, making it susceptible to puncturing the boundary adsorption film and experiencing dry friction, especially at low speeds. Since 0.36 m/s marks the transition point for lubrication states, the subsequent study focuses on the friction and wear behavior of the CPF composites with four different filler contents under constant-speed conditions in both dry and water lubrication conditions.

### 3.2.2. Tribological Behaviors at Constant Sliding Speeds

Figure 4 shows the friction coefficients and wear rates of CPF composites modified with different filler contents under dry friction conditions. It can be seen from Figures 4a and 4c, the addition of g-$C_3N_4$ and $MoS_2$ did not lead to an improvement in tribological performance, as the friction coefficients remained relatively unchanged, and the wear resistance deteriorated. In comparison, the incorporation of Gr can significantly reduce both the friction coefficients and wear rates of the CPF composites (Figure 4b). When the content increased to 10% and 15%, the friction coefficient decreases by 24%, and the wear rate decreases by 78%. As shown in Figure 4d, the addition of h-BN can significantly improve tribological behavior of CPF composites, even with a 3% h-BN content, a substantial 35% reduction in the friction coefficient and 25% decrease in wear rates are achieved. Nonetheless, as the h-BN content increased further to 15%, a subtle trend of rising friction coefficients and wear rates emerged, resembling the behavior of unmodified CPF composites. Therefore, the CPF composites modified with 15% Gr and 3% h-BN have superior tribological properties under dry friction conditions. While the incorporation of g-$C_3N_4$ and $MoS_2$ led to a corresponding increase in the friction coefficient and wear rate of the CPF composites, this result is consistent with the results

Preprints (www.preprints.org) | NOT PEER-REVIEWED | Posted: 20 October 2023 doi:10.20944/preprints202310.1311.v1



of the friction coefficient at low speeds (Figure 3b), indicating that the CPF composites are accompanied by dry friction under low-speed boundary lubrication condition.

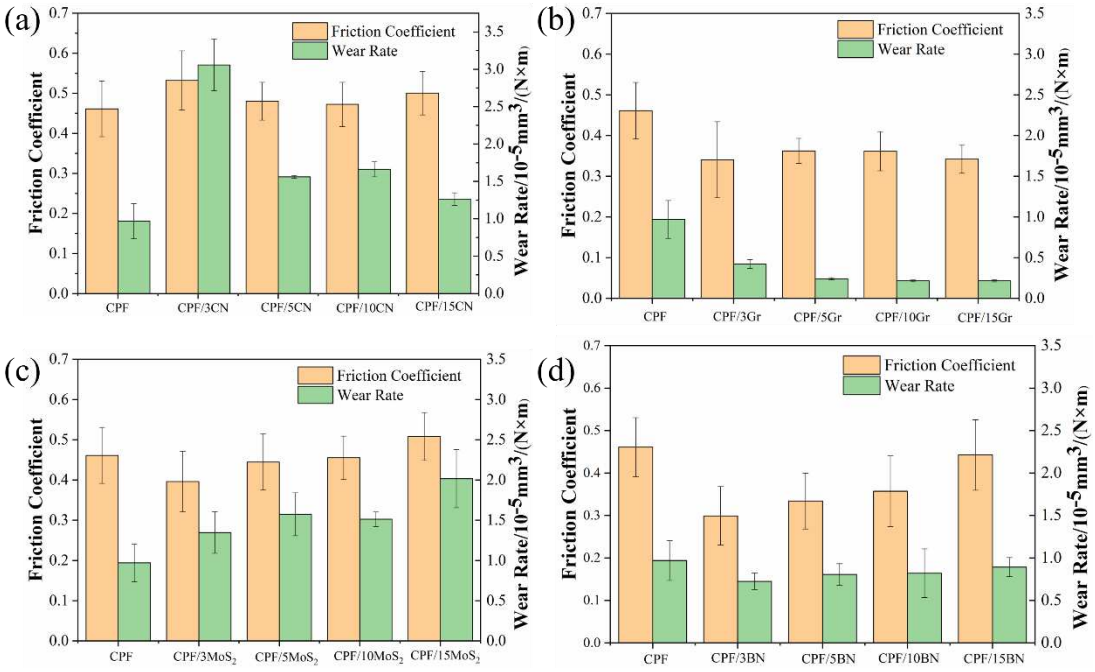


**Figure 4.** Friction coefficients and wear rates of CPF composites modified with different filler contents under dry friction conditions. Load: 132N, revolution speeds: 140rpm.

Figure 5 illustrates the friction coefficients and wear rates of CPF composites modified with varying filler contents under water lubrication, with a load of 132N and a speed of 140rpm. It can be observed that the addition of all four two-dimensional materials lead to a decrease in the friction coefficient compared to unmodified CPF composites, but the changes with increasing content are not significant. By examining the wear rates, it becomes evident that the tribological performance of Gr under water lubrication conditions is notably lower than that under dry friction conditions. Furthermore, as the Gr content increases, the wear rate rises. When the content reaches 15%, the wear amount surpasses that of unmodified CPF composite. Apart from Gr, the other three fillers can reduce the wear rate of the CPF composites, especially 5% h-BN and 10% $MoS_2$, which exhibit the most significant reduction in wear amount. The wear rates are $4.3\times10^{-6}mm^3/Nm$ and $3.54\times10^{-6}mm^3/Nm$, respectively, representing reductions of 47% and 56% compared to unmodified CPF composite. The analysis of friction coefficients and wear rates among the several CPF composites highlights substantial differences in the tribological performance of Gr and $MoS_2$ in different environments.

Preprints (www.preprints.org) | NOT PEER-REVIEWED | Posted: 20 October 2023 doi:10.20944/preprints202310.1311.v1



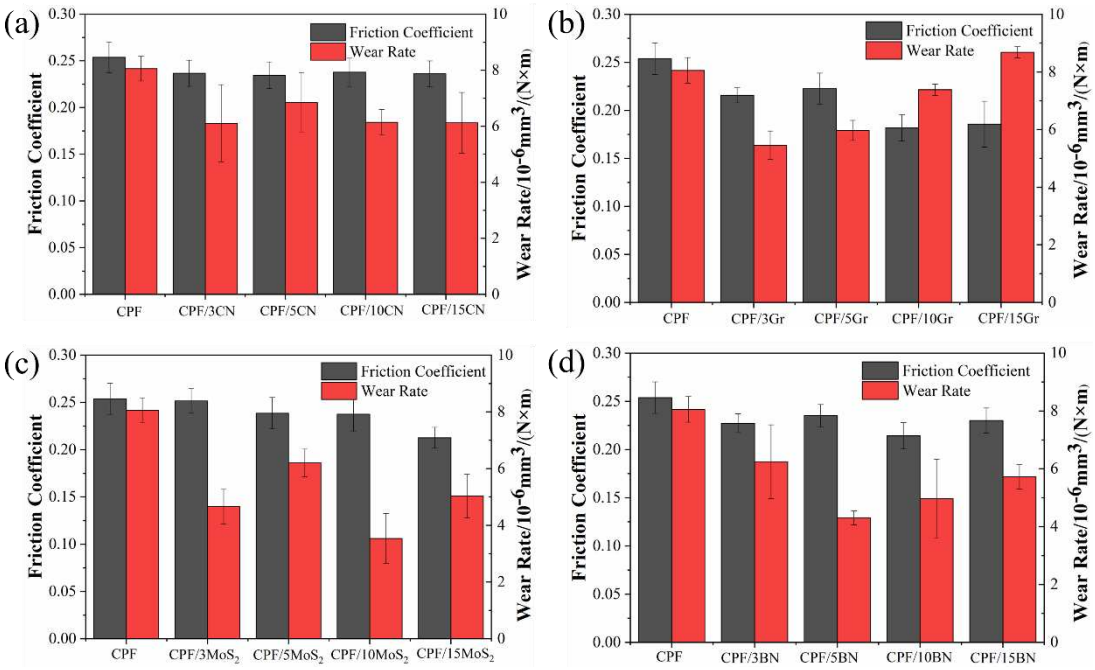


**Figure 5.** Friction coefficients and wear rates of CPF composites modified with different filler contents under water lubrication conditions. Load: 132N, revolution speeds: 140rpm.

The SEM images of the wear surfaces of five CPF composites after dry friction are shown in Figure 6. It can be seen that the wear surface of unmodified CPF composite exhibits slight resin delamination, with the primary wear mechanism being fatigue wear. After adding g-$C_3N_4$ and $MoS_2$, as shown in Figure 6b and 6c, the composites experience significant resin delamination, accompanied by numerous furrows or grooves. The wear debris consists of severed cotton fibers and resin fragments, illustrating a typical abrasive wear mechanism. In contrast, when Gr is introduced, the wear surface is smooth, and there is no apparent resin delamination. It can be attributed to the excellent lubricating properties of Gr[36], as it can transfer to the friction interface during dry friction, leading to a friction reduction and high wear resistance. After the addition of h-BN, only a small number of fatigue cracks appear on the wear surface, and there is no pronounced resin delamination. The wear performance of the composites is improved compared to that with g-$C_3N_4$ and $MoS_2$, but it is inferior to the wear resistance of the CPF composite with Gr added.

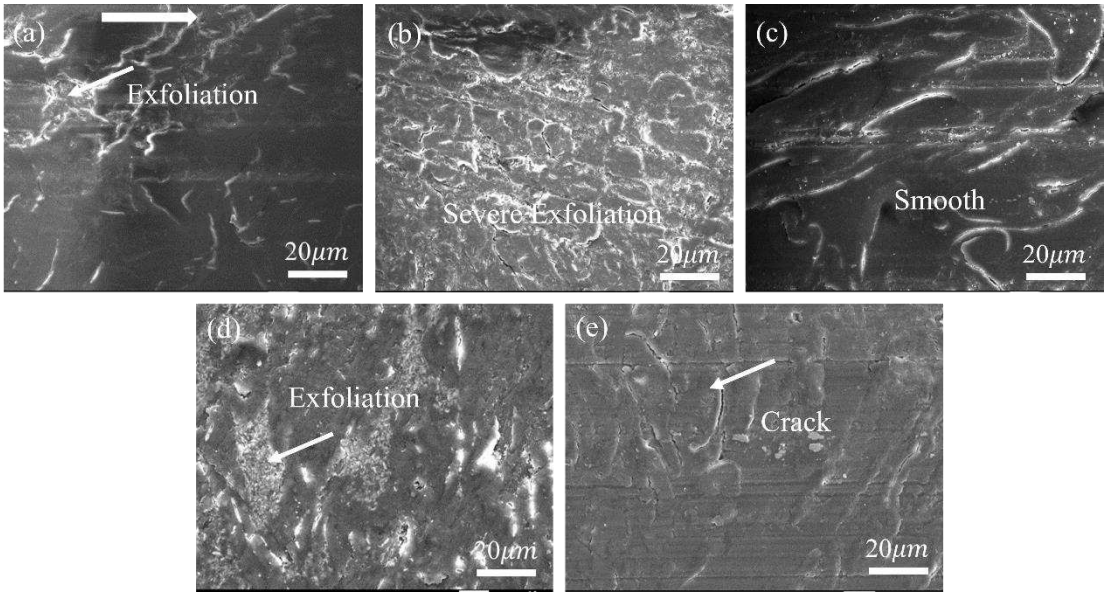

Preprints (www.preprints.org) | NOT PEER-REVIEWED | Posted: 20 October 2023 doi:10.20944/preprints202310.1311.v1



**Figure 6.** SEM images of worn surfaces of (a) CPF, (b) CPF/15CN, (c) CPF/15Gr, (d) CPF/15$MoS_2$, (e) CPF/15BN under dry friction conditions at 132N and 140rpm. Arrows indicate the sliding direction.

Figure 7 demonstrates the SEM images of the worn surfaces of five types of CPF composites under water lubricating condition. As shown in Figure 7a of the unmodified CPF composite, although the surface is smooth, there are many microcracks present. Due to the poor water resistance of phenolic resin, water penetrates into the interior of the composites[37]. During the frictional shear process, they damage the resin/cotton fibers interface, causing it to detach and ultimately develop into cracks. The addition of g-$C_3N_4$ results in a significant reduction in cracks on the worn surface, but resin delamination similar to dry friction conditions still exists（Figure 7b）. After the addition of h-BN, the worn surface shows no significant difference from the unmodified CPF composite except for the reduction in surface cracks (Figure 7e).

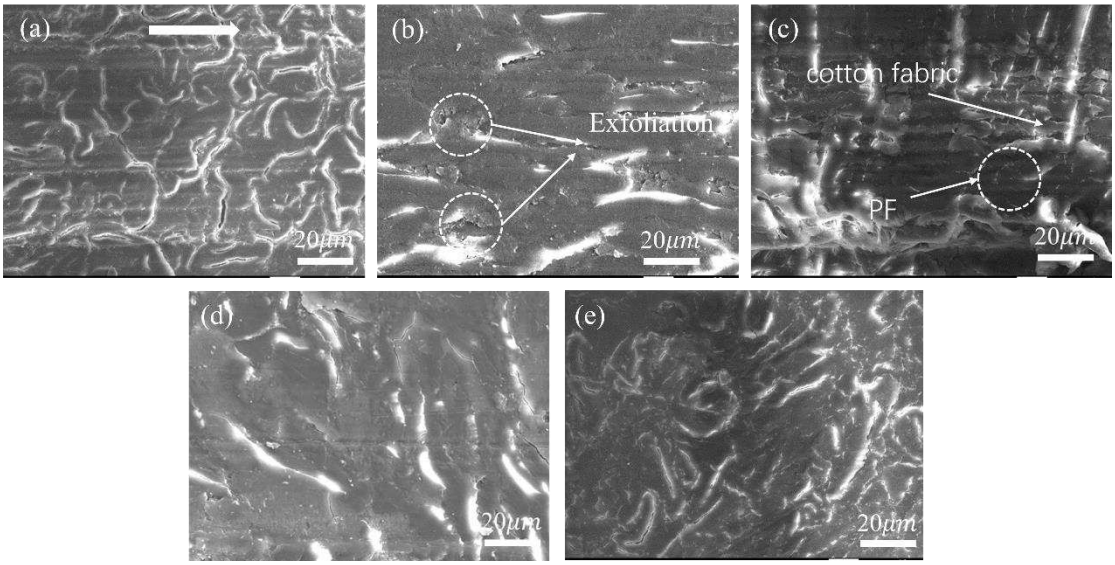


**Figure 7.** SEM images of worn surfaces of (a) CPF, (b) CPF/15CN, (c) CPF/15Gr, (d) CPF/15$MoS_2$, (e) CPF/15BN under water lubrication conditions at 132N and 140rpm. Arrows indicate the sliding direction.

It should be noted that the addition of Gr and $MoS_2$ exhibits a completely different wear morphology from dry friction conditions. The CPF composite modified with Gr does not show a smooth surface similar to dry friction conditions. Instead, there is a significant amount of resin delamination and cotton fibers exposed on the surface. During the friction process, cotton fibers are cut and pulled out, leading to the overall structural damage of the composites (Figure 7c). After the addition of $MoS_2$, the worn surface is smooth, with no obvious cotton fibers exposed on the surface. Resin and cotton fibers jointly withstand the shear stress during the friction process, demonstrating good wear resistance. The wear morphology results are consistent with the wear rate results in Figure 5.

3.2.3. Tribo-Chemistry of Counterpart Surface with Addition of Gr and $MoS_2$

From the above results, it can be seen that Gr and $MoS_2$ modified CPF composites exhibit significant differences in friction and wear performance. CPF/15Gr composite show excellent anti-friction and wear properties under dry friction conditions but have relatively poor wear resistance under wet lubrication conditions. On the other hand, CPF/ 15$MoS_2$ composite demonstrates some wear resistance under wet lubrication conditions, while lacking anti-friction and wear performance under dry friction conditions. In the following, we will focus on the performance differences between the two and analyze their interfacial transfer film morphology and chemical composition, with the aim of revealing their friction and wear mechanisms.

Preprints (www.preprints.org) | NOT PEER-REVIEWED | Posted: 20 October 2023 doi:10.20944/preprints202310.1311.v1



Figure 8 shows SEM images of the counterpart surface morphology after sliding against unmodified CPF, CPF/15Gr, and CPF/15$MoS_2$ composites under dry friction and water lubrication conditions. It can be seen that although a transfer film is formed for the unmodified CPF composite under dry friction, it is thick and discontinuous. This implies that the adhesion of the formed transfer film to the counterpart is relatively weak, making it easily removed during the friction process, leading to a higher wear rate (Figure 8a). After the addition of Gr, the worn surface is relatively smooth, with no apparent resin delamination and fiber exposure (Figure 6c). The formed transfer film is thin and uniform, exhibiting good adhesion to the couple. This prevents direct contact between the couple and the polymer during friction, thereby improving the material's wear resistance (Figure 8b). As shown in Figure 8c, when $MoS_2$ is added as a filler, severe scratching occurs on the counterpart surface, resulting in deep grooves and high surface roughness, increasing the wear of the composites.

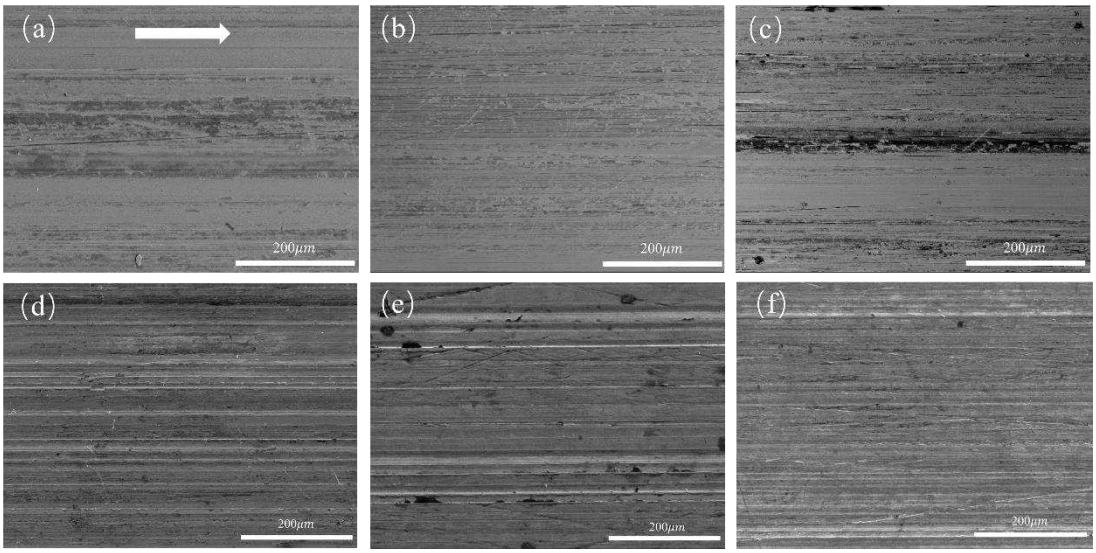


**Figure 8.** SEM images of counterpart surface of (a, d) CPF, (b, e) CPF/15Gr, (c, f) CPF/15$MoS_2$ at 132N and 140rpm; (a-c) under dry friction conditions, (d-f) under water lubrication conditions. Arrows indicate the sliding direction.

Under water lubrication conditions, as shown in Figures 8d-e, the worn surfaces of QSn7-0.2 counterpart after sliding against CPF/15Gr and CPF/15$MoS_2$ composites exhibit completely different morphologies compared to dry friction. The CPF/15Gr composite counterpart surface shows numerous furrows caused by cotton fibers, without a uniform and dense transfer film formation as shown in Figure 8e. In contrast, the CPF/15$MoS_2$ composite counterpart surface has a smooth worn surface with a noticeable presence of transfer film. The worn surface of unmodified CPF composite counterpart surface is similar to the that of CPF/15Gr composite counterpart, also showing a large number of furrows, indicating a similar wear mechanism between the two.

To gain a deeper understanding of the mechanism of frictional chemical reactions, Figure 9 shows XPS spectrum of the counterpart surfaces after sliding against the CPF/15Gr and CPF/15$MoS_2$ composites under dry friction conditions. It can be seen that the counterpart surfaces of Gr and $MoS_2$ exhibit similar C1s spectra. Among them, the feature peak corresponding to 284.6 eV is attributed to C-C bonds, mainly originating from PF, Gr, and cotton fibers. The peak at 286.9 eV corresponds to C-O-C bonds, primarily originating from PF and cotton fibers, while the peak at 288.2 eV corresponds to C=O bonds, originating from cotton fibers (Figures 9a and d). By calculating $I_{C\text{-}C}/I_{C=O}$, it can be seen that the $I_{C\text{-}C}/I_{C=O}$ ratio on the CPF/15Gr composite counterpart surface is higher than that of CPF/15$MoS_2$ composite counterpart surface, indicating the involvement of Gr in the construction of the transfer film on the interface[38, 39]. In the Mo3d spectrum, strong peaks appear at 231.2 eV and 232 eV, corresponding to $MoO_3$, suggesting that $MoS_2$ is oxidized into $MoO_3$ during the friction, resulting in the loss of self-lubricating properties of MOS2[40]. This has an adverse effect on the

Preprints (www.preprints.org) | NOT PEER-REVIEWED | Posted: 20 October 2023 doi:10.20944/preprints202310.1311.v1



friction and wear performance of the CPF composites, leading to higher friction coefficients and wear rates (Figures 9g and e).

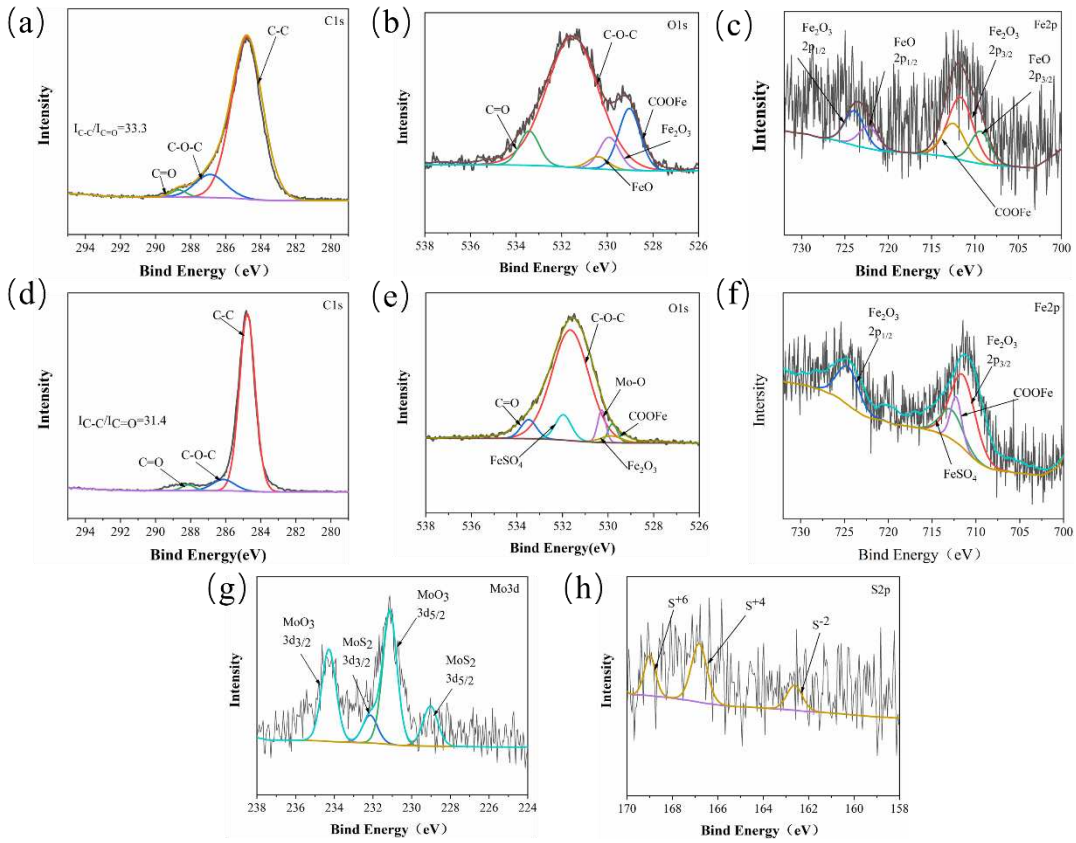


**Figure 9.** XPS spectra of the tribofilm on the worn surface of GCr15 with CPF composites after sliding against under dry friction conditions at 132N, 140 rpm; CPF/15Gr(a-c), CPF/15$MoS_2$（d-h）.

Comparing the O1s spectra of the two, a strong peak at 529.1 eV, corresponding to the presence of organometallic compounds, appeared on the CPF/15Gr composite counterpart surface. Due to the shear forces and frictional heat, molecular chain breakage occurs in the phenolic resin and cotton fibers, resulting in the formation of polymer carbon radicals. These carbon radicals can react with $O_2$ and $H_2O$ in the air and ultimately react with the Fe present in the coupling, leading to the generation of organometallic compounds[41]. The formation of organometallic compounds is beneficial for enhancing the bond strength between the transfer film and the coupled surface, thereby better utilizing their lubrication and wear-resistant properties[38]. It can be seen from Figure 9e, a significant amount of Mo is oxidized into $MoO_3$, and S elements can also react with the Fe in the coupling, generating $FeSO_4$ (Figure 9e). It should be noted the presence of reactive Mo and S elements inhibits the occurrence of chelation reactions, leading to the low intensity of organometallic compounds.

XPS spectra of the counterpart surface after sliding against the CPF/15Gr and CPF/$MoS_2$ composites under water lubrication conditions is shown in Figure 10. Similar to Figure 9, the carbon peak is almost the same. However, the intensity of $I_{C-C}/I_{C=O}$, especially for CPF/15Gr composite, is significantly lower compared to dry friction conditions, indicating the ability to form a transfer film on the friction interface is weaker in the presence of water. Observing the O1s spectra of both, in contrast to dry friction, there is no evidence of chelation compound formation on the counterpart, indicating that under water lubrication conditions, the necessary conditions for chemical reactions seen in dry friction are not present. This leads to weaker adhesion between the transfer film and the counterpart. Furthermore, it can be seen that characteristic peaks corresponding to Mo-S at 228.9 eV and 232.7 eV in the Mo3d spectrum, as well as the corresponding feature peak $S^{-2}$ at 162.4 eV in the S2p spectrum, indicates that under water lubrication conditions, $MoS_2$ has not undergone oxidation,

Preprints (www.preprints.org) | NOT PEER-REVIEWED | Posted: 20 October 2023 doi:10.20944/preprints202310.1311.v1



thereby preserving its self-lubricating properties. Therefore, the CPF/15$MoS_2$ composite exhibits better tribological performance compared to CPF/15Gr composite under water lubrication conditions.

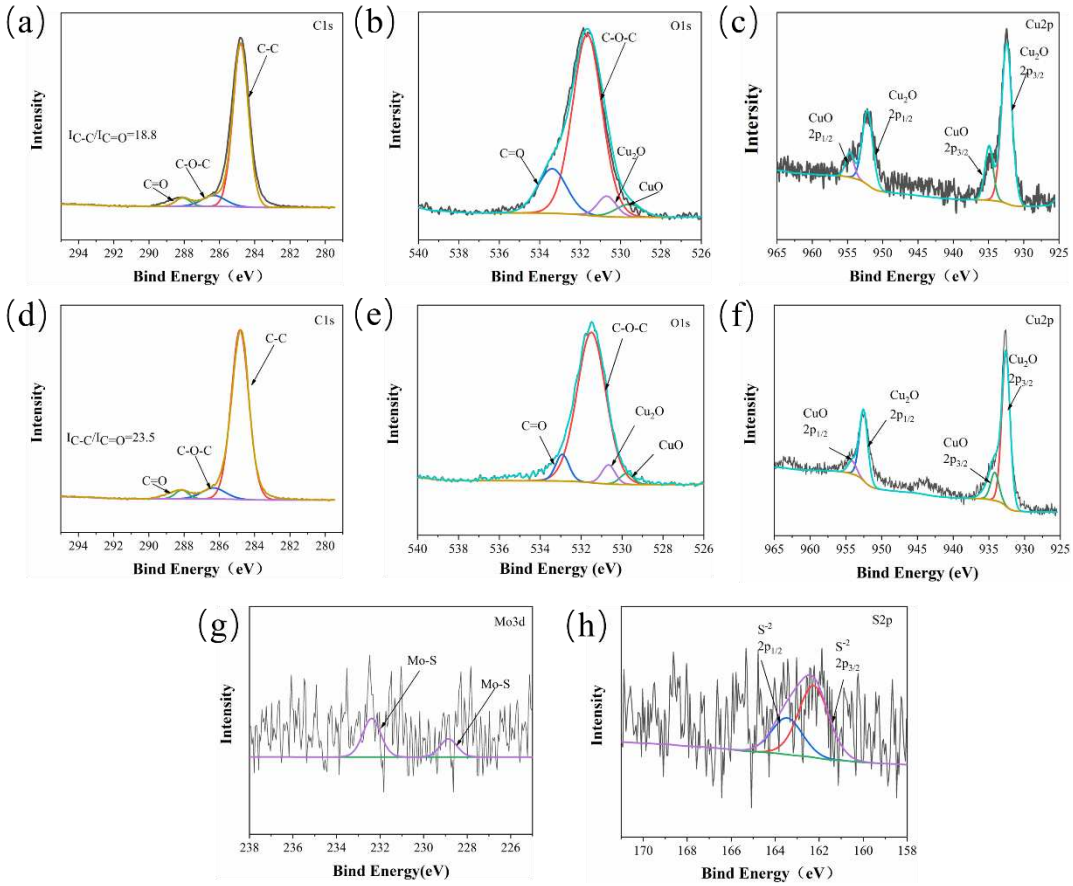


**Figure 10.** XPS spectra of the tribofilm on the worn surface of QSn7-0.2 with CPF composites after sliding against under water lubrication conditions at 132N, 140 rpm; CPF/15Gr(a-c), CPF/15$MoS_2$（d-h）.

### 3.2.4. Molecular Dynamics Simulation of CPF Composites Modified by Gr and $MoS_2$

Based on the above analysis, the differences in the tribological performance of CPF/Gr and CPF/$MoS_2$ composites under dry friction and water lubrication conditions primarily stem from the formation of high-performance transfer films. The adsorption capability between the material and the counterpart directly influences the material's transfer[42]. In the following, molecular dynamics simulations were used to investigate the adsorption behavior of PF, Gr, and $MoS_2$ on the counterpart under both air and water environments. It can better explain the difference in tribological properties of the two materials in different environments. The main components of GCr15 and QSn7-0.2 are Fe and Cu, so Fe and Cu were chosen as friction layer of the molecular models of counterpart[43]. The model system consists of PF, cotton fabric, Gr, and MoS2, as shown in Figure 11.

Preprints (www.preprints.org) | NOT PEER-REVIEWED | Posted: 20 October 2023 doi:10.20944/preprints202310.1311.v1



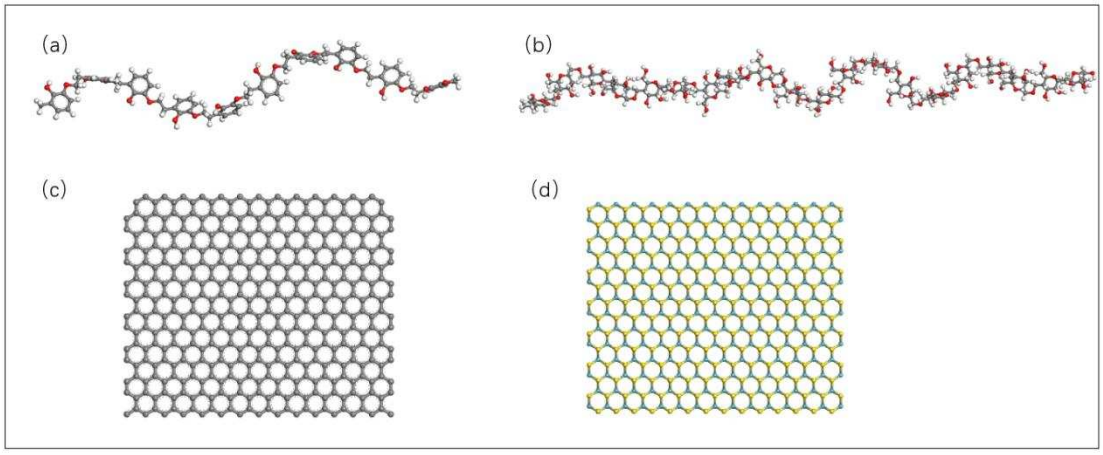


**Figure 11.** molecular models of (a) PF, (b) cotton fabric, (c) Gr, (d) $MoS_2$.

The amorphous cell module was used to construct the amorphous cell of the CPF composites, and it was optimized as shown in Figure 12. The calculations were performed using the NVT ensemble with zero total momentum, the Universal force field, the Nose temperature control method to maintain the temperature at 300K (simulating room temperature), a van der Waals force cutoff radius of 12.5 Å (1 Å = 0.1 nm), and a Coulomb force accuracy of 0.01 Kcal·mol$^{-1}$. The time step for calculations was set to 0.5 fs, and the simulation time was 100 ps. Adsorption energy calculations were then performed on the optimized model using the following formula[44]:

$$E=-E_{inter}=E_{total}-\ (E_{layer1}-E_{layer2}) \quad (2)$$

where E is the adsorption energy, $E_{inter}$ is the interaction energy between the CPF composite and counterpart surface, $E_{layer1}$ is the interaction between the CPF composite and $E_{layer2}$ is the interaction energy of the counterpart surface, unit Kcal/mol.

Preprints (www.preprints.org) | NOT PEER-REVIEWED | Posted: 20 October 2023 doi:10.20944/preprints202310.1311.v1



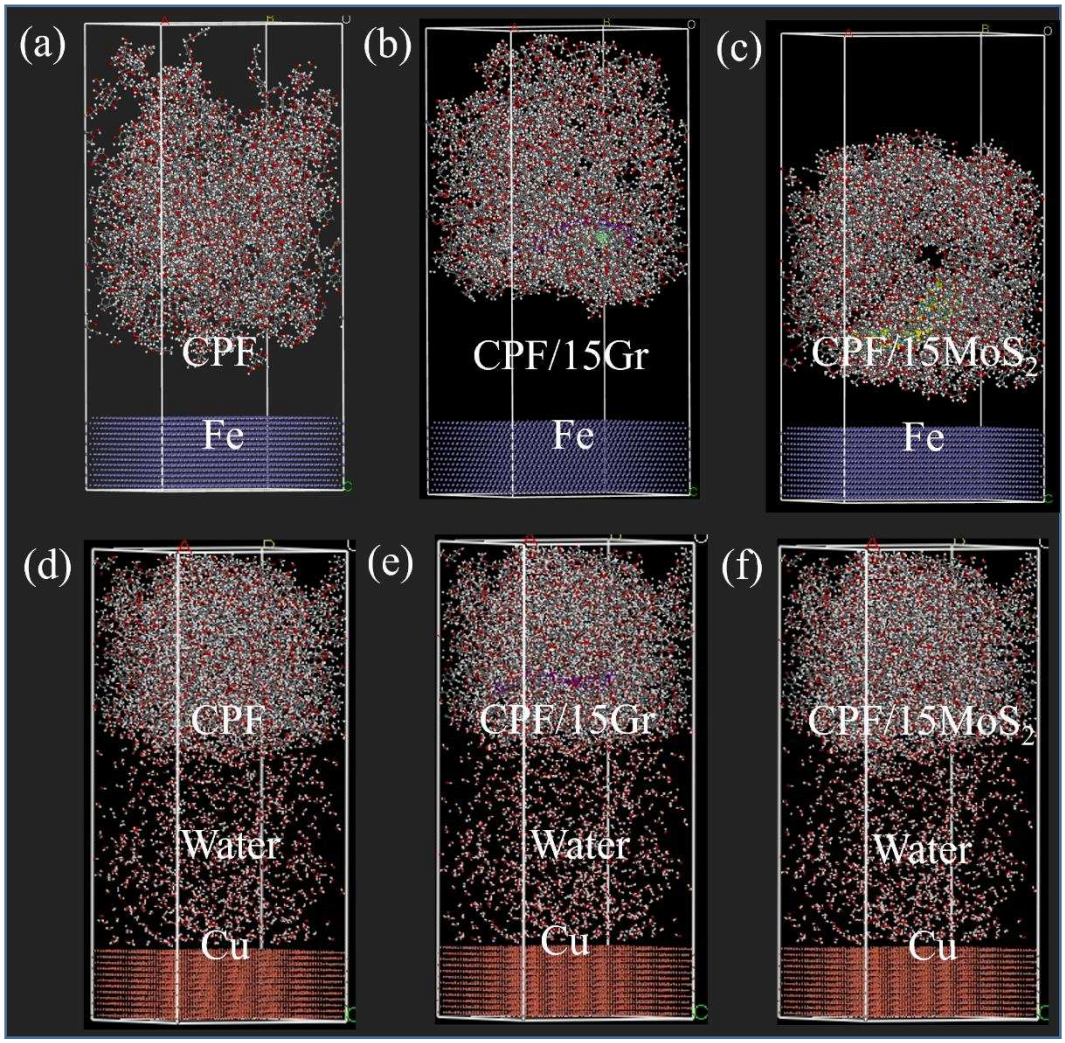


**Figure 12.** CPF composites adsorption model under different lubrication conditions; (a-c) under dry friction conditions, (d-f) under water lubrication conditions.

The adsorption energy of the optimized model is calculated as shown in Tables 2,3.

**Table 2.** Adsorption energy of three CPF composites under dry friction conditions.

| | $E_{total}$ | $E_{layer1}$ | $E_{layer2}$ | E |
|---|---|---|---|---|
| CPF | 22063.98 | 22129.34 | -42.6215 | 22.7391 |
| CPF/15Gr | 59974.35 | 60044.69 | -42.6215 | 27.7161 |
| CPF/ 15$MoS_2$ | 38583.75 | 38650.52 | -42.6215 | 24.1535 |

**Table 3.** Adsorption energy of three CPF composites under water lubrication conditions.

| | $E_{total}$ | $E_{layer1}$ | $E_{layer2}$ | E |
|---|---|---|---|---|
| CPF | 24527.14 | 20324.73 | 4227.439 | 25.0309 |
| CPF/15Gr | 52501.46 | 48298.61 | 4227.439 | 24.589 |
| CPF/15$MoS_2$ | 44046.73 | 39845.03 | 4227.439 | 25.7347 |

It can be seen that there is adsorption between the CPF composites and the counterpart. Under dry friction conditions, Gr exhibits a higher adsorption energy. This suggests that under dry friction conditions, the adsorption between Gr and the Fe counterpart further promotes the formation and stable presence of the transfer film. This prevents direct contact at the friction interface, leading to effective lubrication and wear resistance. Under water lubrication conditions, the adsorption energies

Preprints (www.preprints.org) | NOT PEER-REVIEWED | Posted: 20 October 2023 doi:10.20944/preprints202310.1311.v1



of both $MoS_2$ and PF have increased, while the adsorption energy of Gr is lower than that under dry friction conditions. This indicates that the adsorption capacity of Gr to the counterpart is weaker under water lubrication conditions, which is not beneficial to the formation of a transfer film. As a result, the tribological performance decreases compared to dry friction conditions.

### 3.2.5. The Synergistic Interaction between $MoS_2$ and Gr

The earlier analysis indicates that CPF/Gr and CPF/$MoS_2$ composites are suitable for working under dry friction and water lubrication conditions, respectively. The reason for this lies in whether a self-lubricating transfer film has formed on the friction interface. To verify if there is good synergistic lubrication between the two fillers, a design was proposed to add both fillers together to prepare corresponding CPF composites. Subsequently, the friction coefficients and wear rates were tested under dry friction and water lubrication conditions.

As shown in Figure 13, the CPF/15Gr/15$MoS_2$ composite exhibits good tribological performance under both dry friction and water lubrication conditions. Under dry friction conditions, there is a 30% reduction in the friction coefficient and a 63% decrease in the wear rate when compared to unmodified CPF composite. Under water lubrication conditions, the friction coefficient decreases by 16%, and the wear rate decreases by 41%. The combination of both fillers preserves the excellent tribological performance of Gr under dry friction conditions and maintains the self-lubricating properties of $MoS_2$ under water lubrication conditions. This demonstrates that $MoS_2$ and Gr have excellent synergistic lubrication effects.

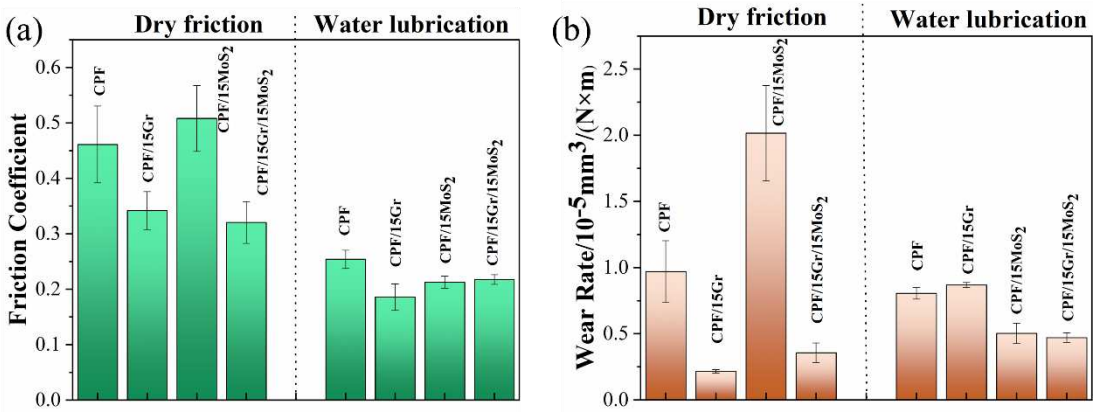


**Figure 13.** (a) Friction coefficients, (b) wear rates of CPF, CPF/15Gr, CPF/15$MoS_2$ and CPF/15Gr/15$MoS_2$ at 132N and 140rpm.

## 4. Conclusions

The tribological performance of CPF composites modified with g-$C_3N_4$, Gr, $MoS_2$ and h-BN under both dry friction and water lubrication conditions were studied. The main conclusions are as follows:

1. Gr exhibits significantly better tribological performance than the other three fillers under dry friction. When the Gr content increased to 10% and 15%, the friction coefficient decreases by 24%, and the wear rate decreases by 78% compared to unmodified CPF composite.
2. Under water lubrication conditions, all four fillers did not significantly alter the friction coefficient of the CPF composites. However, except for an excessive amount of Gr, the other three fillers can reduce the wear rate of the composite material. Particularly, in the case of 5% h-BN and 10% $MoS_2$, the wear rate decreased by 47% and 56%, respectively.
3. The adsorption capacity between the composites and the counterpart plays a crucial role in the formation of the transfer film under both dry friction and water lubrication conditions. Calculations of adsorption energy reveal that Gr is well-suited for dry friction, while $MoS_2$ is more suitable for operation in a water environment. Using both $MoS_2$ and Gr as co-modifiers for CPF composite, effective synergistic lubrication can be achieved.

Preprints (www.preprints.org) | NOT PEER-REVIEWED | Posted: 20 October 2023 doi:10.20944/preprints202310.1311.v1



**Acknowledgments:** This work was resourced by Key Research and Development Program of Shandong Province (2023CXPT060), National Natural Science Foundation (52175199, 52105225), and Youth Innovation Promotion Association of Chinese Academy of Sciences (Grant No. 2020417). We are also grateful to Key Science and Technology Program of Gansu Province (22ZD6GA002), and Key Program of the Lanzhou Institute of Chemical Physics, CAS (No. KJZLZD-1).

**Conflicts of Interest:** The authors declare no conflict of interest.

## Reference

1. Xie X, Guo Z,Yuan C. Investigating the water lubrication characteristics of sisal fiber reinforced ultrahigh-molecular-weight polyethylene material[J], Polymer Composites, 2020, 41(12): 5269-5280.
2. Huang J, Zhou X, Wang J, et al. Influence of temperature on friction of polymeric materials in water[J], Wear, 2019, 426-427: 868-876.
3. Zhou G, Li P, Liao D, et al. The Friction-Induced Vibration of Water-Lubricated Rubber Bearings during the Shutdown Process[J], Materials (Basel), 2020, 13(24).
4. Chen J, Guo Z, Li X, et al. Development of gradient structural composite for improving tribological performance of PU material in water-lubricated bearings[J], Tribology International, 2022, 176.
5. Zhang L, Guo Y, Xu H, et al. A novel eco-friendly water lubricant based on in situ synthesized water-soluble graphitic carbon nitride[J], Chemical Engineering Journal, 2021, 420.
6. Li Z, Ma S, Zhang G, et al. Soft/Hard-Coupled Amphiphilic Polymer Nanospheres for Water Lubrication[J], ACS Appl Mater Interfaces, 2018, 10(10): 9178-9187.
7. Guo Z, Dong S, Yang Z, et al. Tribological Properties of Aramid Fiber-Microcapsule Modified Ultra-high Molecular Weight Polyethylene Composites for Water Lubrication[J], Journal of Materials Engineering and Performance, 2022, 31(7): 6000-6008.
8. Dong C, Yuan C, Wang L, et al. Tribological Properties of Water-lubricated Rubber Materials after Modification by $MoS_2$ Nanoparticles[J], Sci Rep, 2016, 6: 35023.
9. Wang C, Bai X, Dong C, et al. Friction properties of polyacrylamide hydrogel particle/HDPE composite under water lubrication[J], Polymer, 2019, 180.
10. Gao C, Guo G, Zhang G, et al. Formation mechanisms and functionality of boundary films derived from water lubricated polyoxymethylene/hexagonal boron nitride nanocomposites[J], Materials & Design, 2017, 115: 276-286.
11. Holmberg K,Erdemir A. Influence of tribology on global energy consumption, costs and emissions[J], Friction, 2017, 5(3): 263-284.
12. Liu Y, Gao G, Jiang D, et al. Enhancement of Underwater Tribological Properties of Hybrid PTFE/Nomex Fabric Laminate Composites by Epoxy Resins[J], ACS Omega, 2022, 7(9): 7737-7744.
13. Ren G, Zhang Z, Song Y, et al. Effect of MWCNTs-GO hybrids on tribological performance of hybrid PTFE/Nomex fabric/phenolic composite[J], Composites Science and Technology, 2017, 146: 155-160.
14. Ren G, Zhang Z, Zhu X, et al. Combined effect of air-plasma treatment and lubricant filling on the dry sliding wear behavior of hybrid PTFE/Nomex fabric/phenolic composite[J], Composites Science and Technology, 2014, 100: 204-211.
15. Zhang Z, Yang M, Yuan J, et al. Friction and wear behaviors of $MoS_2$-multi-walled-carbonnanotube hybrid reinforced polyurethane composite coating[J], Friction, 2018, 7(4): 316-326.
16. Liu Y, Gao G, Jiang D, et al. Enhancement of the Water-Lubricated Tribological Properties of Hybrid PTFE/Nomex Fabric Laminate Composite via Epoxy Resin and Graphite Filler[J], Materials (Basel), 2021, 15(1).
17. He Y, Duan R, Zhang Q, et al. Reinforce the mechanical toughness, heat resistance, and friction and wear resistance of phenolic resin via constructing self-assembled hybrid particles of graphite oxide and zirconia as nano-fillers[J], Advanced Composites and Hybrid Materials, 2021, 4(2): 317-323.
18. Zhou S, Wang F, Chen J, et al. Enhanced mechanical, thermal, and tribological performance of 2D-laminated molybdenum disulfide/RGO nanohybrid filling phenolic resin composites[J], Advanced Composites and Hybrid Materials, 2022, 5(2): 1206-1220.
19. Renda C G,Bertholdo R. Study of phenolic resin and their tendency for carbon graphitization[J], Journal of Polymer Research, 2018, 25(11).
20. Jiang P, Wang Z, Liu H, et al. Improving the strength and oxidation resistance of phenolic resin derived pyrolytic carbons via Cu-catalyzed in-situ formation of $SiC@SiO_2$[J], Solid State Sciences, 2021, 118.
21. Li C, Zhang J, Yi Z, et al. Preparation and characterization of a novel environmentally friendly phenol–formaldehyde adhesive modified with tannin and urea[J], International Journal of Adhesion and Adhesives, 2016, 66: 26-32.

Preprints (www.preprints.org) | NOT PEER-REVIEWED | Posted: 20 October 2023 doi:10.20944/preprints202310.1311.v1




22. Yuan J, Zhang Z, Yang M, et al. Coupling hybrid of BN nanosheets and carbon nanotubes to enhance the mechanical and tribological properties of fabric composites[J], Composites Part A: Applied Science and Manufacturing, 2019, 123: 132-140.
23. Zang C, Xing Y, Yang T, et al. The Preparation and Wear Behaviors of Phenol-Formaldehyde Resin/BN Composite Coatings[J], Polymers (Basel), 2022, 14(19).
24. Zhang H-J, Zhang Z-Z,Guo F. Studies of the Influence of Graphite and $MoS_2$ on the Tribological Behaviors of Hybrid PTFE/Nomex Fabric Composite[J], Tribology Transactions, 2011, 54(3): 417-423.
25. Oliver B A, Dong Q, Ramezani M, et al. Tribological Performance of Bamboo Fabric Reinforced Epoxy Composites[J], Macromolecular Materials and Engineering, 2023.
26. Yu P, Zhang D, Zhang L, et al. Significance of g-$C_3N_4$ nanosheets for enhancing tribological performance of epoxy subjected to starved lubrication[J], Tribology International, 2022, 174: 107762.
27. Zhang L, Qi H, Li G, et al. Significantly enhanced wear resistance of PEEK by simply filling with modified graphitic carbon nitride[J], Materials & Design, 2017, 129: 192-200.
28. Wu L, Zhang Z, Yang M, et al. One-step synthesis of g-$C_3N_4$ nanosheets to improve tribological properties of phenolic coating[J], Tribology International, 2019, 132: 221-227.
29. Ren G, Zhang Z, Zhu X, et al. Influence of lubricant filling on the dry sliding wear behaviors of hybrid PTFE/Nomex fabric composite[J], Journal of Materials Science, 2014, 49(10): 3716-3724.
30. Wu H, Yin S, Du Y, et al. Alkyl-Functionalized Boron Nitride Nanosheets as Lubricant Additives[J], ACS Applied Nano Materials, 2020, 3(9): 9108-9116.
31. Levita G, Restuccia P,Righi M C. Graphene and MoS2 interacting with water: A comparison by ab initio calculations[J], Carbon, 2016, 107: 878-884.
32. Hou X, Bai P, Li J, et al. $MoS_2$ reinforced PEEK composite for improved aqueous boundary lubrication[J], Friction, 2023.
33. Yang J, Zhang H, Chen B, et al. Fabrication of the g-$C_3N_4$/Cu nanocomposite and its potential for lubrication applications[J], RSC Advances, 2015, 5(79): 64254-64260.
34. Chen B, Wang J,Yan F. Friction and Wear Behaviors of Several Polymers Sliding Against GCr15 and 316 Steel Under the Lubrication of Sea Water[J], Tribology Letters, 2011, 42(1): 17-25.
35. Gao C P, Guo G F, Zhao F Y, et al. Tribological behaviors of epoxy composites under water lubrication conditions[J], Tribology International, 2016, 95: 333-341.
36. Tan H, Guo Y, Wang D, et al. The development of a Cu@Graphite solid lubricant with excellent anti-friction and wear resistant performances in dry condition[J], Wear, 2022, 488-489.
37. Pavlidou S,Papaspyrides C D. The effect of hygrothermal history on water sorption and interlaminar shear strength of glass/polyester composites with different interfacial strength[J], Composites Part A: Applied Science and Manufacturing, 2003, 34(11): 1117-1124.
38. Yu P, Li G, Zhang L, et al. Role of SiC submicron-particles on tribofilm growth at water-lubricated interface of polyurethane/epoxy interpenetrating network (PU/EP IPN) composites and steel[J], Tribology International, 2021, 153.
39. Xu Y, Peng Y, Dearn K D, et al. Synergistic lubricating behaviors of graphene and $MoS_2$ dispersed in esterified bio-oil for steel/steel contact[J], Wear, 2015, 342-343: 297-309.
40. You Y-L, Li D-X, Si G-J, et al. Investigation of the influence of solid lubricants on the tribological properties of polyamide 6 nanocomposite[J], Wear, 2014, 311(1-2): 57-64.
41. Guo L, Zhang G, Wang D, et al. Significance of combined functional nanoparticles for enhancing tribological performance of PEEK reinforced with carbon fibers[J], Composites Part A: Applied Science and Manufacturing, 2017, 102: 400-413.
42. Longlong L N P B Z. Tribological Performance of PTFE/FeOCl Composites under Paraffin-lubricated Conditions[J], Tribology Letters, 2023.
43. Xu M, Wang X, Wang T, et al. Ag nanoparticle decorated graphene for improving tribological properties of fabric/phenolic composites[J], Tribology International, 2022, 176.
44. Wang J. Water lubrication bearing technology and application [M][J], Beijing: Science Press, 2018.


**Disclaimer/Publisher's Note:** The statements, opinions and data contained in all publications are solely those of the individual author(s) and contributor(s) and not of MDPI and/or the editor(s). MDPI and/or the editor(s) disclaim responsibility for any injury to people or property resulting from any ideas, methods, instructions or products referred to in the content.